Numerical Methods in Civil Engineering

Journal Homepage: https://nmce.kntu.ac.ir/

Numerical assessment of the influences of uplift pressure in joints on the seismic response of an arch dam having a jointed foundation

Hasan Mostafaei[*], Mohammadreza Mashayekhi[**], Nilupa Herath[***] and Muhammad Ali Rostampour[****]

ARTICLE INFO

RESEARCH PAPER

Article history:
Received:
October 2022.
Revised:
December 2022.
Accepted:
December 2022.

Keywords:
Uplift pressure;
Jointed foundation;
Nonlinear finite element;
Wedge;
Arch dam.

Abstract:

Joints, which are usually located in the abutments of dams, play a vital role in the seismic stability evaluation of arch dams. This paper presents a comprehensive numerical investigation of the influence of uplift pressure in joints on the seismic response of an arch dam, with a focus on the interaction between the dam and the rock wedges. For this study, the Bakhtiari arch dam, having one rock wedge at each abutment, was chosen as a case study, and three distinct finite element models of the dam were developed. Three components of El Centro were applied to the dam's foundation, and the influences of dam-rock wedge interaction on the crest displacement time history and tensile damage of the arch dam were investigated. Four different scenarios were taken into account. The results indicated that taking uplift pressure in joints into account has important effects on the dam responses.

1. Introduction

Dams are vital infrastructure that play a critical role in water resource management, serving multiple purposes such as water storage for irrigation, flood control, hydroelectric power generation, and water supply for domestic, industrial, and recreational use [1, 2]. Constructed of materials such as concrete, earth, and rock, dams are designed to withstand the forces of water and the environment. The consequences of a dam failure can be catastrophic, leading to loss of human life, severe property damage, and significant environmental and economic impacts [3-5]. Therefore, it's essential for dam owners and operators to take the necessary precautions to prevent dam failures and to regularly assess the stability of the structures [6]. A wide variety of approaches can be used to gain a comprehensive understanding of a dam's performance and safety, such as finite element method [7-11], and extended finite element method [12, 13].

Concrete arch dams are a type of dam that transfers the forces they encounter to their abutments. This design allows the dam to be much thinner than other types of dams, making it a cost-effective solution. Due to the geometry requirements, concrete arch dams are required to maintain stability in their abutments. It was found that the main cause of these type of dam failures is the instability of their abutments [14]. Due to the importance of accurate analyses of abutments' stability, many studies have been conducted to explore the effective parameters on abutments' stability by employing different approaches [15, 16]. In the following section, some related studies which have carried out around the world are briefly mentioned.

Londe developed the limit equilibrium method to investigate the stability of rock wedges in 1973 [17]. Nowadays, this method is used at the initial stages of dam designs. The main advantage of this method over other common stability analysis methods is that it uses a simple quantity such as the safety factor. In another study, Londe investigated the Malpasset dam failure [18]. They concluded that due to the

[1] *Research Assistant, Department of Civil Engineering, Isfahan University of Technology, Isfahan, Iran. Email: h.mostafaei@cv.iut.ac.ir*

[*2] *Corresponding author. Assistant Professor, Department of Civil Engineering, K.N. Toosi University of Technology, Tehran, Iran (Corresponding Author). Email: m.mashayekhi@kntu.ac.ir*

[3] *Lecturer, Department of Infrastructure Engineering, University of Melbourne, Melbourne, Australia. Email: nherath@unimelb.edu.au*

[4] *Research Assistant, Department of Civil Engineering, Isfahan University of Technology, Isfahan, Iran. Email: ma.rostampour@cv.iut.ac.ir*

https://doi.org/10.52547/NMCE.2212.1000

application of the thrust force, which was parallel to the layering of the left abutment, the penetration of the layers significantly decreased and reached 1% of the initial value. This phenomenon made the bedrock act like an underground dam. With the decrease in permeability, proper drainage was not done, and the pore uplift pressure was increased as much as the entire reservoir head. Therefore, a wedge rupture was formed. Sliding the rock wedge and the structure around the right abutment led to the dam's failure.

Using finite element analysis, Witke presented his failure hypothesis of the Malpasset dam by considering dam-foundation interaction and the stresses resulting from seepage on the foundation [19, 20]. His theory was similar to that of Londe, but there was a difference of opinion on the problem of cracking on the upstream face of the sliding rock wedge. Londe indicated that the tensile stresses in the direction perpendicular to the bedrock at the upstream face of the dam were caused by the thrust forces. However, Witke showed that the tensile stresses in the direction perpendicular to the bedrock at the upstream face of the dam were caused by the hydrostatic pressure. In Londe's theory, the interaction of the abutment and the dam was ignored. The loads applied to the block through the body were calculated using the trial load method, while in Witke's hypothesis, finite element analysis allowed redistribution of forces, resulting in reliable and accurate results.

The effects of the slope of the grout curtain on the dam's response using the finite element method were studied by Erban and Gell [21]. The abutment was considered to be crossed by three series of discontinuities. He indicated that the tensile stress at the interface of a dam and the foundation decreased when the slope of the grout curtain rose. Moreover, the most suitable slope of the grout curtain is 70 degrees.

In 2017, Mostafaei et al. [15, 22] presented a computer software named ASADAM by using Visual Basic to investigate the pseudo-static and dynamic stability of rock wedges. Their research showed that rotating the applied horizontal acceleration had a significant impact on the safety factor of the rock wedges, and ignoring the rotation of applied acceleration in the horizontal plane leads to errors. Also, by comparing the results obtained from dynamic and quasi-static analysis, they indicated that quasi-static analysis is more conservative than dynamic analysis. Also, in another study, they investigated the effect of uplift pressure on the safety factor of the rock wedges by considering six different scenarios of uplift pressure. The results showed that the grout curtain performance significantly influenced the safety factor of dams' abutments.

Joints in the foundation are experienced uplift pressure during earthquakes. This uplift pressure is of a key importance in the stability of dams' abutments and may jeopardize the stability of dams. To the authors' best knowledge, no study in the scientific literature investigated the effects of uplift pressure on the response of dams having jointed foundations. Therefore, in this research, an attempt is made to assess the influences of uplift pressure on the seismic response of the dam, taking into account the dam-wedge interaction. To this end, four different scenarios were considered. In these scenarios, uplift pressure in joints vary from 25% to 100%. Based on this, the Bakhtiari concrete arch dam with a wedge in each abutment of the dam has been selected as a case study. A 3-D finite element model was developed to simulate the behavior of the dam-reservoir-foundation interaction. In this finite element model, the foundation is modeled as a mass medium with infinite elements at the truncated boundary conditions to prevent the wave from returning to the model. A boundary condition has been applied at the end of the reservoir so that the waves moving away from the structure are completely absorbed, and no return waves occur from the end.

2. Finite element model

During past decades, many efforts have been made to assess the seismic behavior of concrete dams subjected to seismic loading. The assessment is based on the capability of the user-defined constitutive models to describe the structural behavior. In this regard, different crack models have been proposed to simulate the nonlinear seismic behavior of concrete arch dams under strong ground motions with the help of numerical methods. Abaqus FEA [23], as a commercial finite element software package employed in the current research, provides various types of concrete constitutive models, such as the discrete crack model, the smeared crack model, and the concrete damage plasticity (CDP) model [23]. In this study, the seismic response of an arch dam with a jointed foundation was studied using the Abaqus software package [23]. The CDP, capable of modelling concrete's inelastic behavior, is used in this study. The following sections address some important information about concrete behavior, boundary conditions, concrete damaged plastic, and contact property used in the study.

2.1 Behavior of concrete

Stress-strain behavior of concrete in tension and compression are used to predict the behavior of the structure until failure and after failure. Since the laboratory results of used concrete are not available [24], Kent and Park's model, which has two ascending and descending branches in compression, was used to model the nonlinear behavior of concrete. The constitutive law for concrete based on the Kent-Park is illustrated in Figure 1. In this figure, f'_c and ε_{co} stand for the compressive strength of concrete and corresponding strain, respectively. f_c and ε_c are the axial stress and strain of concrete. ε_{co} is equal to 0.002.

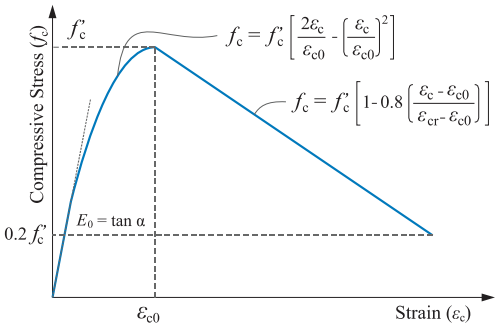

Fig. 1: Kent and Park's stress-strain curve for the behavior of concrete in compression.

For concrete in tension, two ascending and descending lines are assumed. Linear-elastic stress-strain behavior is considered up to concrete tensile strength. The post-failure behavior of concrete is modeled using a linear stress-strain relationship. It should be mentioned that the tensile failure strain was taken as 10 times the cracking strain (ε_{cr}), as shown in Figure 2.

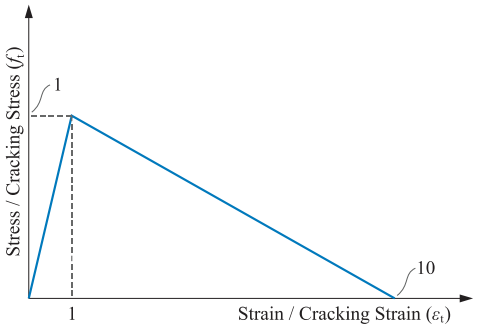

Fig. 2: The stress-strain behavior of concrete in tension.

2.2 Concrete Damage Plasticity (CDP) Model

The complex mechanical behavior of concrete is described by adopting the Concrete Damage Plasticity (CDP) model as the material constitutive model. The CDP model was introduced theoretically by Lubliner et al. [25] and modified by Lee and Fenves [26]. This model assumes two failure mechanisms of the concrete material: compressive crushing and tensile cracking. The stress-strain relationships of concrete subjected to uniaxial compressive and tensile loading are presented in Figure 3.

According to Figure 3, after unloading on the strain softening branch of the stress-strain curves, the elastic stiffness of the material appears to be damaged (degraded). This is defined by two damage variables in tension (d_t) and in compression (d_c) that are assumed to be functions of inelastic strain. The damage variables, d_t and d_c, are increasing functions of the equivalent inelastic strain, varying from zero to one. A value of zero indicates the material without damage, and a value of one indicates the loss of the total resistance of the material. The uniaxial stress-strain relationships in the tension and compression regions of concrete can be expressed as follows:

$$\sigma_t = (1-d_t)E_0(\varepsilon_t - \varepsilon_t^{pl}) \quad (1)$$

$$\sigma_c = (1-d_c)E_0(\varepsilon_c - \varepsilon_c^{pl}) \quad (2)$$

where E_0 is the initial (undamaged) elastic stiffness of the concrete, and ε_t^{pl} and ε_c^{pl} are the equivalent plastic strains of concrete. Moreover, damage parameters, d_t and d_c, can take the values from zero to one, indicating the undamaged and fully damaged materials, respectively.

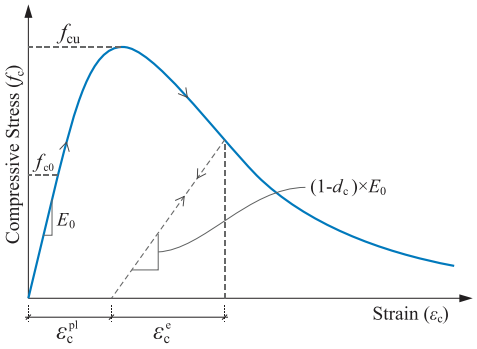

(a) Uniaxial compression

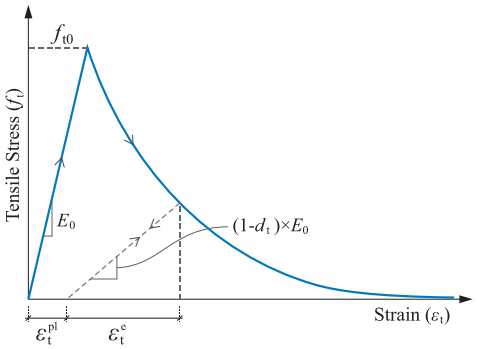

(b) Uniaxial tension

Fig. 3: The stress-strain behavior of concrete.

2.3 Infinite element

By considering the mass of the foundation, boundary conditions should be applied to the far end of the foundation. In boundary problems, in order to apply the conditions around the foundation, the infinite element was used. In dynamic analysis, infinite elements generate additional shear and normal stresses at the boundaries of finite elements, which are proportional to the shear and normal components of boundary velocity. These are determined as the damping constants of the boundary to minimize the reflection of the energy of compression and shear waves into the boundary of the finite elements. Herein, CIN3D8R was employed.

2.4 Contact surface

In the scientific literature, joints were modeled using spring or interface elements [27]. Joints are a special contact between the two surfaces with tangential and normal behaviors [28]. Researchers usually use hard contact. In this behavior, the two surfaces are in contact when the normal force between them is compressive [5]. In other words, when

the normal force is tensile, two surfaces separate from each other. It should be mentioned that the tensile strength of joints was neglected. The stresses transmitted through contact surfaces are related to each other by the Coulomb friction model, which can be expressed as follows:

$$\tau_u = \mu\sigma \tag{3}$$

where τ_u, σ, and μ stand for the shear stress, normal stress, and friction coefficient, respectively. Moreover, to consider the delamination at the contact surface, a bilinear traction-separation law is defined in Abaqus. The separation can be caused due to normal and shear stresses, which can be defined in three directions independently. Before the first damage, the linear behavior that relates the normal and shear stresses to the corresponding separations across the contact surface can be defined as follows:

$$\mathbf{t} = \begin{Bmatrix} t_n \\ t_s \\ t_t \end{Bmatrix} = \begin{bmatrix} K_{nn} & K_{ns} & K_{nt} \\ K_{ns} & K_{ss} & K_{st} \\ K_{nt} & K_{st} & K_{tt} \end{bmatrix} \begin{Bmatrix} \delta_n \\ \delta_s \\ \delta_t \end{Bmatrix} = \mathbf{K\delta} \tag{4}$$

where **t**, **δ** and **K** are the nominal traction stresses, separation vectors and elastic constitutive matrix, respectively. The term **t** includes three components t_n, t_s, and t_t representing the normal and the two shear tractions, respectively. Moreover, the corresponding separations are introduced by δ_n, δ_s, and δ_t, respectively. Also, due to ignoring the tensile strength of joints, K_{nn} was set to be nil. By considering the uncoupled elastic behavior of traction-separation, the non-diagonal members were set to be zero. When load increases, the shear and normal stresses across the interface rise. As the damage initiation criterion is met, the cohesive bond can experience damage. In this study, the damage initiation criterion was defined based on the quadratic stress criterion, which can be expressed as follows [29]:

$$\left(\frac{\langle t_n \rangle}{t_{n0}}\right)^2 + \left(\frac{t_s}{t_{s0}}\right)^2 + \left(\frac{t_t}{t_{t0}}\right)^2 = 1 \tag{5}$$

where t_{n0}, t_{s0}, and t_{t0} stand for the peak values of the contact stress in normal, the first and second shear directions, respectively. Moreover, "⟨ ⟩" in represents the Macaulay bracket which filters out the compressive stress. It is worth noting that damage occurs when the quadratic interaction function reaches a value of one. By ignoring tensile contact stress, the damage initiation criterion is the only function of the tangential contact stress state (t_s and t_t) at the interface. The damage initiation criterion can be written as follows:

$$\left(\frac{t_s}{t_{s0}}\right)^2 + \left(\frac{t_t}{t_{t0}}\right)^2 = 1 \tag{6}$$

As damage progresses, the cohesive stiffness gradually degrades. A linear softening traction-separation is taken into account for this process, as shown in Figure 4.

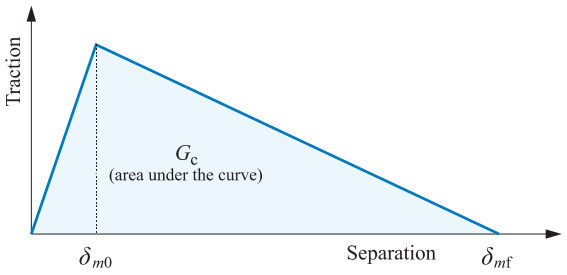

Fig. 4: The bilinear traction-separation law.

The damage at the contact point, D, monotonically varies from zero to one. The shear stresses affected by the damage in the absence of the normal stiffness can be expressed as follows:

$$t_s = (1-D)\bar{t}_s \tag{7}$$

$$t_t = (1-D)\bar{t}_t \tag{8}$$

where $\bar{t}_s$ and $\bar{t}_t$ are the tangential contact stresses, calculated by assuming the elastic traction-separation behavior for the current separation without taking the damage into account. Also, an effective separation, δ_m, can be obtained by combining two shear-separation components across the interface as follows:

$$\delta_m = \sqrt{\delta_s^2 + \delta_t^2} \tag{9}$$

The fracture energy, which is the required energy to result in complete bond failure, can be obtained by the area under the bilinear traction-separation law (Figure 4). The complete failure criterion in the zero-normal-stiffness can be expressed as follows:

$$\left(\frac{G_s}{G_{sc}}\right)^2 + \left(\frac{G_t}{G_{tc}}\right)^2 = 1 \tag{10}$$

where G_i and G_{ic} (i=s, t) are the s- or t-components of work done by the traction with their conjugate separations and the critical fracture energies required to cause failure, respectively. The evolution of the damage variable for linear softening can be calculated as follows:

$$D = \frac{\delta_{mf}\left(\delta_{m\max} - \delta_{m0}\right)}{\delta_{m\max}\left(\delta_{mf} - \delta_{m0}\right)} \tag{11}$$

where $\delta_{m\,\max}$ stands for the maximum value of the effective separation, which is obtained during the loading history.

3. Model description

The Bakhtiari dam, a doubly curve arch dam located in Iran, was selected as a case study to assess the impact of uplift pressure in the joints on the seismic behavior dam by considering wedge-dam interaction. The dam's height and crest length are 325 and 534 m, respectively [30]. It is worth noting that the dam's thickness varies from 66.3 m at the base to 8 m at the crest. The normal level-water of the reservoir is 320 m. For more accurate results, the length of the

reservoir was assumed to be three times the dam's height. It is noteworthy that if the water length-to-dam height ratio is assumed to be three, the responses of the model will be reliable [31]. The material properties of dam concrete, foundation rock, and water are presented in Table 1.

Table 1: Material properties of concrete, rock and water.

Material	Density (kg/m^3)	Elastic modulus (GPa)	Poisson ratio
Dam concrete	2400	24	0.18
Foundation rock	2600	12	0.25
Water	1000	-	-

It is also worth mentioning that the bulk modulus of water is considered equal to 2.2 GPa. Figure 5 shows the stress-strain curve of concrete for compressive and tensile loading of concrete.

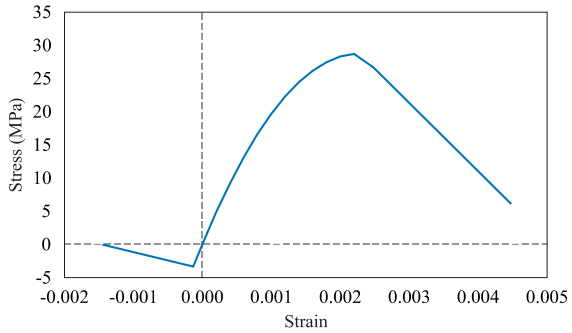

Fig. 5: Concrete stress-strain curve based on the Kent and Park model.

The material damping of rock and concrete was achieved based on the Rayleigh damping. It should be noted that mass-proportional and stiffness-proportional coefficients were equal to 0.6002 and 0.0239, respectively.

Three discontinuous planes are crossed in each dam abutment, creating wedges. The geometry of wedges is indicated in Figure 6. The mechanical and geometrical properties of these discontinuous planes, named P1, P2 and P3 are listed in Table 2. It is worthwhile noting that the volume of wedge in left and right banks are 2.396×10^6 m^3 and 5.318×10^6 m^3, respectively.

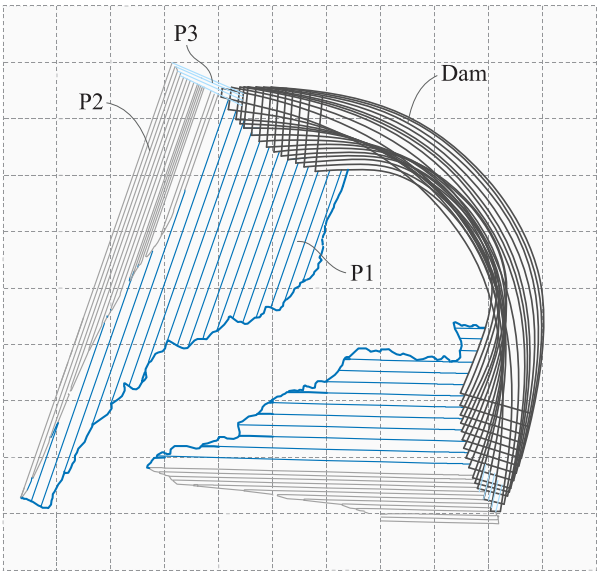

Fig. 6: The geometry of the wedges.

For seismic analysis of the dam, the ground acceleration time histories of Imperial Valley earthquakes (El Centro) were considered [32]. The time histories of the Imperial Valley earthquake are illustrated in Figure 7. It is worthwhile noting that three components of the ground acceleration earthquakes are applied simultaneously.

Table 2: Mechanical and geometrical parameters of the wedges.

Parameters	Wedges					
	Left abutment			Right abutment		
	P1	P2	P3	P1	P2	P3
Uplift force (MN)	11,432	39,453	14,042	37,687	42,357	29,315
Area (m^2)	23,514	54,974	9,720	46,244	60,159	19,407
Unit normal vector	(0,0,1)	(0.75, -0.61, 0.26)	(0.33, 0.92, -0.23)	(0,0,1)	(-0.82, -0.51, 0.26)	(-0.48, 0.83, -0.11)

3-D finite element models which include the dam, the wedges, the reservoir, and the rest of the foundation are developed in Abaqus. It is worth noting that 5440 eight-node acoustic elements (AC3D8R) with pressure degrees of freedom at each node were used to model the reservoir. It is worth mentioning that the pressure at the reservoir's surface was considered to be zero. Also, the boundary conditions at the end of the reservoir were taken into account for the complete absorption of the hydrodynamic wave. Moreover, 21982 eight-node elements (C3D8R) were used to model the dam's foundation.

For the finite element model of a concrete arch dam in Abaqus, the infinite element is typically used to represent the far-field boundary condition, such as the upstream or downstream face of the foundation of the dam. By using the infinite element, the influence of this far-field boundary condition on the rest of the model can be taken into account in the analysis. Also, the transmitting boundary condition is used to couple the truncated finite element model to an equivalent continuous domain that represents the remainder of the reservoir. This allows the finite element model to accurately capture the behavior of the entire reservoir, including the effects of reflections and transmissions of

waves at the boundary of the truncated model. The transmitting boundary condition is an important tool for modelling fluid-structure interactions, wave propagation, and other problems involving fluid flow in truncated reservoirs.

To investigate the effects of wedge modelling on the response of the dam, the joints are modelled as the boundary separating the wedge from the foundation. Three separate finite element models were developed, as shown in Figure 8.

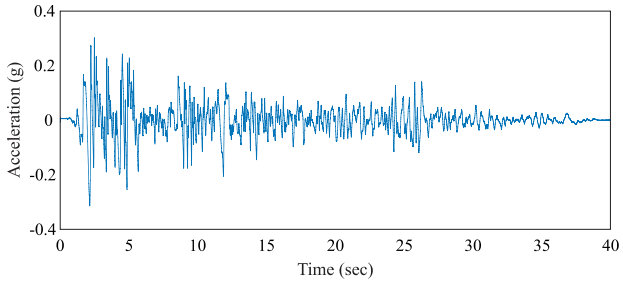

(a) Stream direction

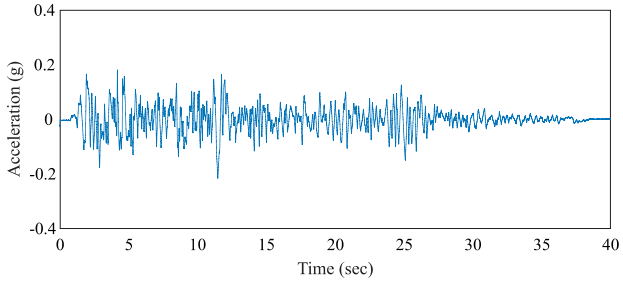

(b) Cross-stream direction

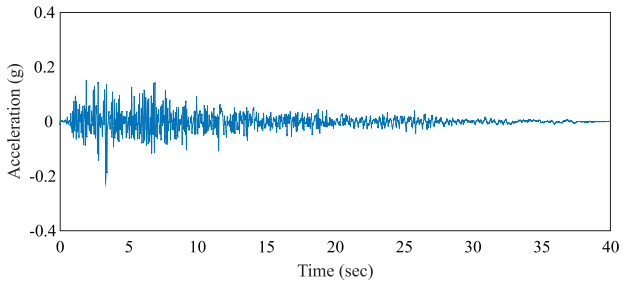

(c) Vertical direction

Fig. 7: Time history of El Centro accelerogram.

3.1 Contact behavior

In this study, the friction coefficient is assumed as 1. It is worthwhile mentioning that the value of tangential hardness is considered to be $K_{ss} = K_{tt} = 56$ GPa/m [29]. Also, according to the conducted research, the shear key is equal to one-tenth of the compressive strength of rock ($t_{s0} = t_{t0} = 3.0$ MPa) is considered as the criteria for the beginning of sliding [33]. Also, the effective slip at the moment of damage was assumed to equal to $\delta_{m0} = 53.6\times10^{-6}$ m. Also, the final effective slip was assumed to be six times the initial effective slip, $\delta_{mf} = 321.6\times10^{-6}$ m [29]. By taking these values into account, the fracture energy was equal to $G_c = 0.482\times10^{-3}$ MPa, as indicated in Figure 9.

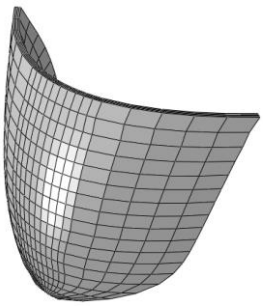

(a) Dam

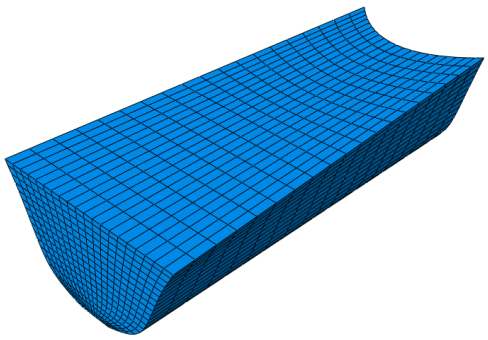

(b) Reservoir

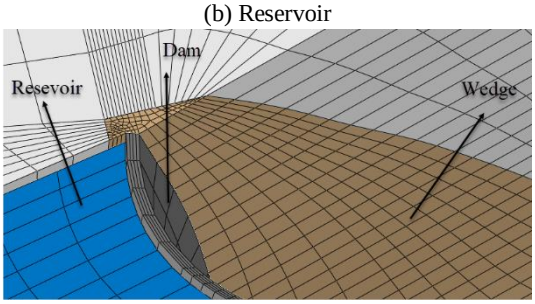

(c) Foundation having left wedge

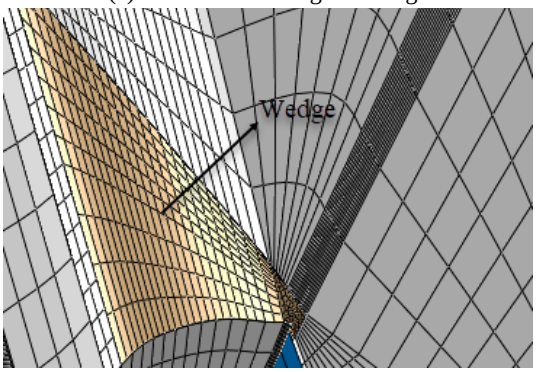

(d) Foundation having right wedge

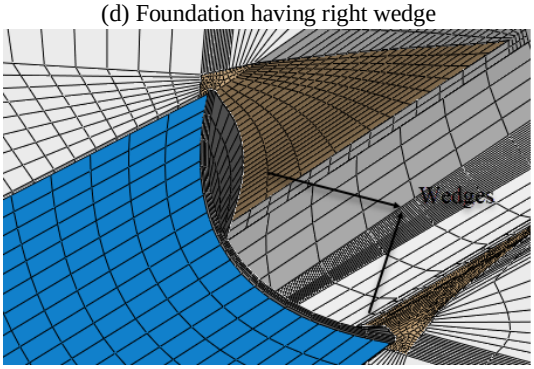

(e) Foundation having both the left and right wedges

Fig. 8: Finite element model.

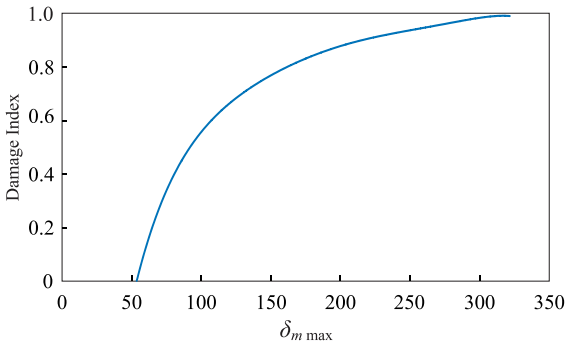

Fig. 9: The evolution of the damage variable.

3.2 Uplift pressure in joints

One of the most important steps in the design of dams is sealing the dam's abutments. The most common sealing method is the grout curtain to reduce the amount of seepage to an acceptable level and increase the dam's stability. Parameters like borehole spacing, rock permeability, grout's density and pressure significantly affect the grout curtain performance [33]. The seepage and uplift pressure problem have been observed right after the first impounding in a wide variety of dams [33, 34]. To investigate the performance of the grout curtain on the response of the jointed dam, four different scenarios were considered. In these scenarios, the uplift force was considered a percentage of the total uplift force, calculated in the absence of the grout curtain and taking the head of water into account. The mentioned percentages are 25%, 50%, 75%, and 100% for scenario 1 to 4, respectively. In these scenarios, 100% and 25% indicate poor and good grout curtain performance, respectively.

4. Results and discussions

4.1 Wedge in the left abutment

The time histories of crest displacement in stream direction for different scenarios of hydrostatic pressure are shown in Figure 10. It can be concluded that the increase in uplift pressure in the joints when they are open has a significant effect on the seismic response of the dam. As the uplift pressure applying to joints is large enough, the seismic response of the dam increases dramatically.

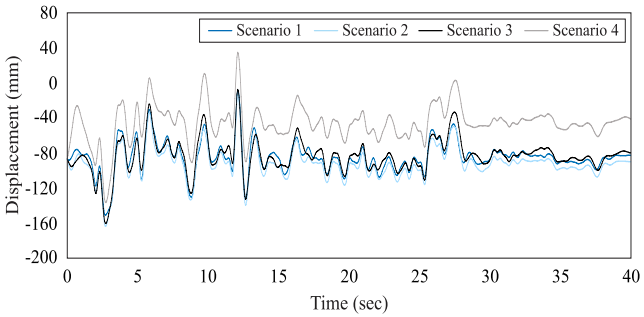

Fig. 10: Time histories of displacement at the crest of the dam having wedge at left abutment midpoint for different scenarios in the stream direction.

Furthermore, the displacement contours of the dam at the moment of maximum displacement are shown in Figure 11. The results show that the maximum displacements are in the vicinity of the left abutment. In contrast, according to the author's experience, the maximum displacement of the dam occurs in the central part of the dam. It is also worth noting that due to the large displacement of the dam, the interfaces between the wedge and foundation experience damage.

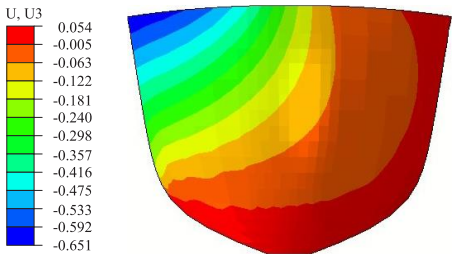

(a) Scenario 1

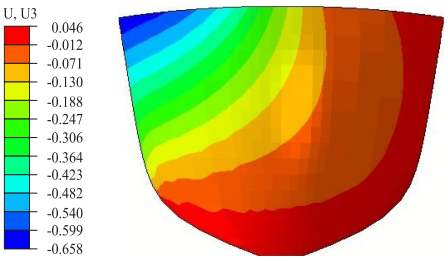

(b) Scenario 2

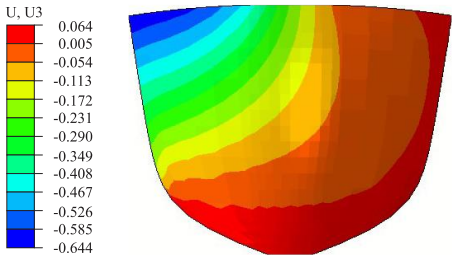

(c) Scenario 3

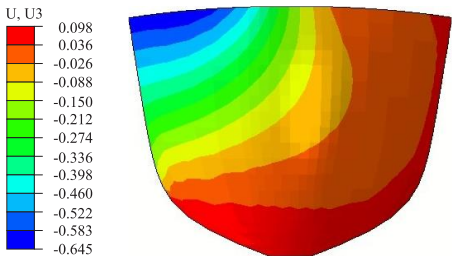

(d) Scenario 4

Fig. 11: The contour of relative displacement of the dam with a wedge at the left abutment for different scenarios.

The contour of tensile damage at the upstream and downstream faces of the dam is shown in Figure 12. The results illustrated that the uplift pressure in joints could cause severe damages to the body of the dam. These damages started at the level of the P1 plane, which indicates that the other two planes are open, and cracks grow vertically. Moreover, an increase in hydrostatic pressure results in cracks propagating toward the center part of the dam.

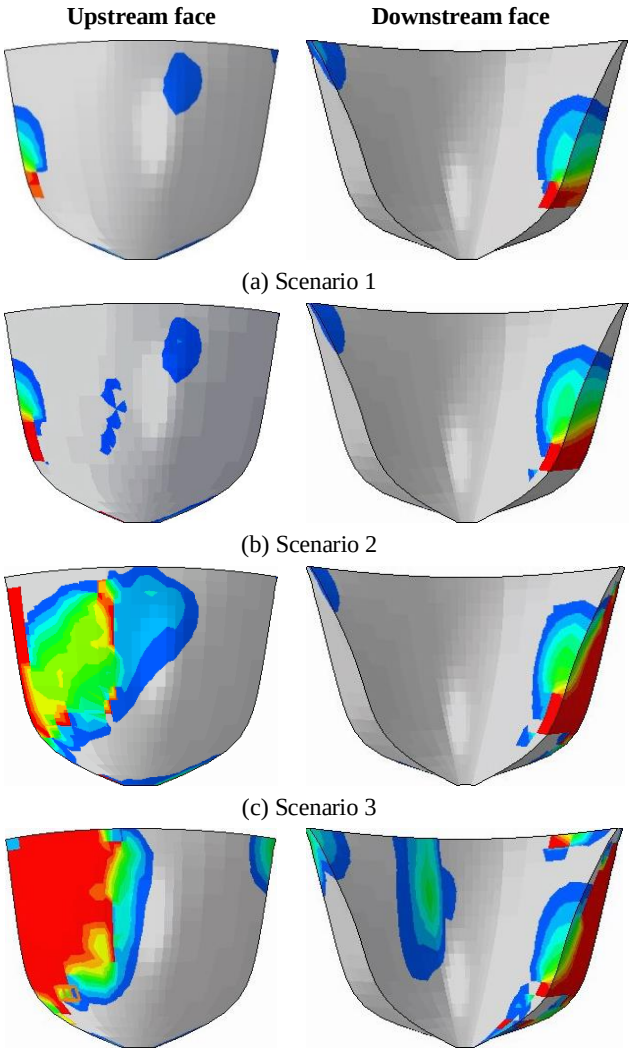

(a) Scenario 1

(b) Scenario 2

(c) Scenario 3

(d) Scenario 4

Fig. 12: The contour of tensile damage of the dam having a wedge at the left abutment for different scenarios.

4.2 Wedge in the right abutment

Based on different scenarios of hydrostatic pressure, Figure 13 illustrates the time history of crest displacement in stream direction. As a result, the crest displacement has an ascending trend concerning the pressure in the joints. Besides, when enough strong pressure is applied to joints, the dam experiences large displacements.

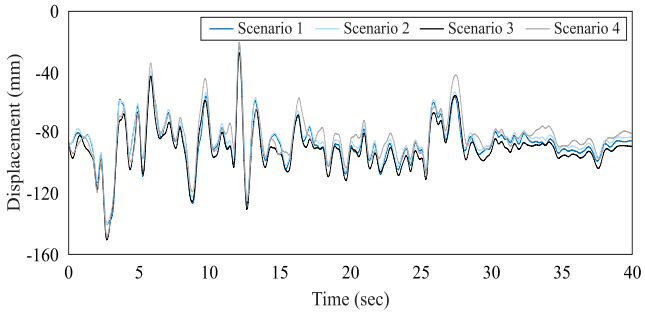

Fig. 13: Time histories of relative displacement at the crest of the dam having a wedge at the right abutment midpoint for different scenarios in the stream direction.

Furthermore, Figure 14 illustrates the dam's displacement contour at maximum displacement. Based on the results, the maximum displacement occurs near the right abutment, while the author's experience suggests the maximum displacement occurs in the middle of the dam. It can be seen that the displacement of the dam is more inclined towards the right abutment.

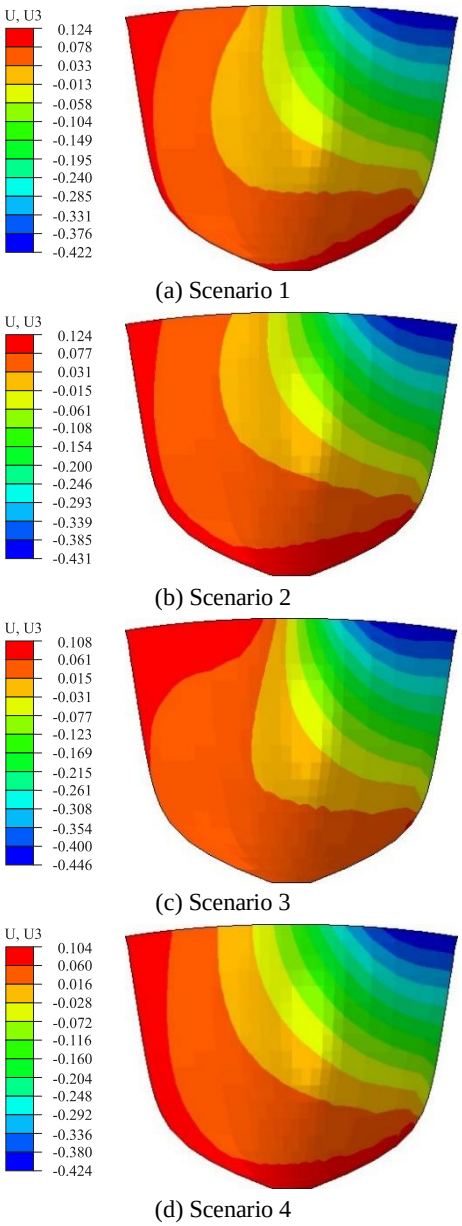

(a) Scenario 1

(b) Scenario 2

(c) Scenario 3

(d) Scenario 4

Fig. 14: The contour of displacement of the dam with a wedge at the right abutment for different scenarios.

Figure 15 presents the tensile damage contour of the dam for different scenarios of hydrostatic pressure. The results show that the severity of tensile damage of the dam increases when the pressure in the joints rises.

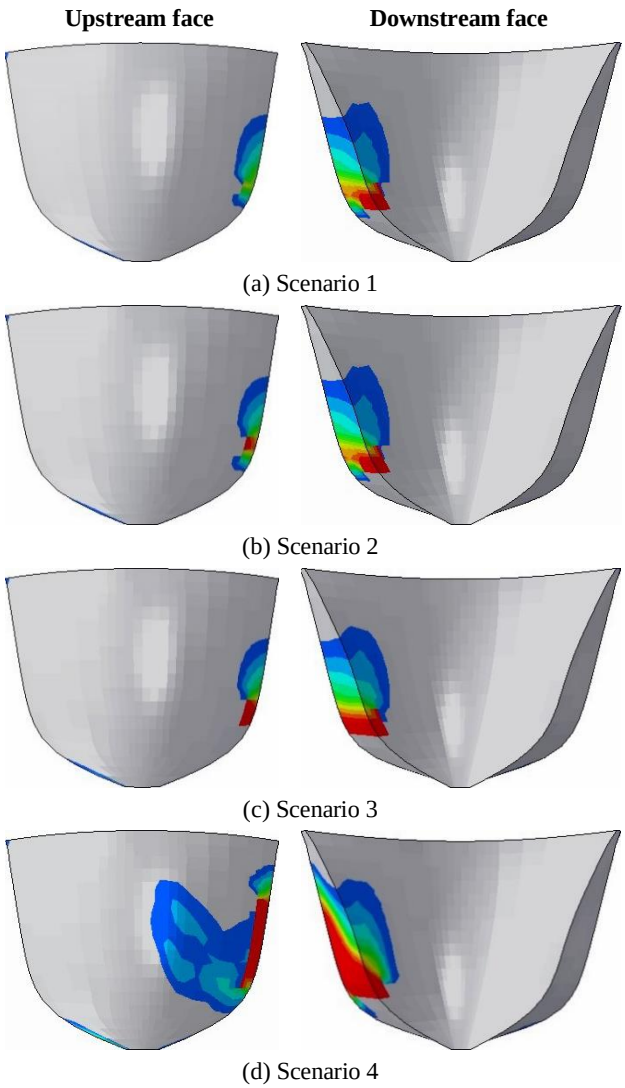

(a) Scenario 1

(b) Scenario 2

(c) Scenario 3

(d) Scenario 4

Fig. 15: The contour of tensile damage of the dam having a wedge at the right abutment for different scenarios.

In addition, by comparing the results obtained for the dam having a wedge in the left abutment and those achieved for the dam with the wedge in the right abutment, it can be inferred that the tensile damage in the former is more severe than the latter. The difference between the degrees of tensile damage of the two models may be due to the fact that the wedge in the right abutment is heavier than the one in the left abutment.

4.3 Wedges in both abutments

Figure 16 illustrates the displacements of crests in stream direction under different hydrostatic pressure scenarios shown over time. There is a significant influence on the seismic response of the dam when the joints are open. An increase in the uplift pressure on joints leads to a rise in the dam's seismic response.

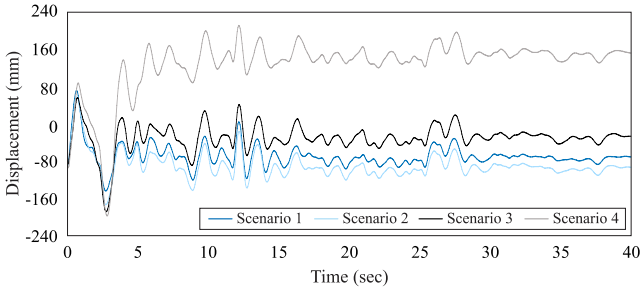

Fig. 16: Time histories of relative displacement at the crest of the dam having wedges at both abutments for different scenarios in the stream direction.

Besides, the contours of the dam's displacement at the moment that displacement becomes maximum are indicated in Figure 17. It can be inferred that the maximum displacement occurs in the central part of the dam.

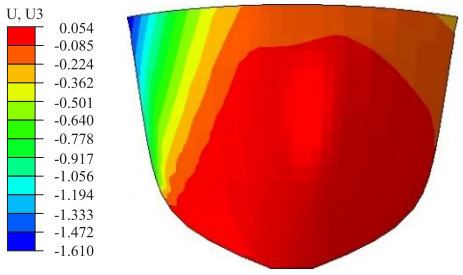

(a) Scenario 1

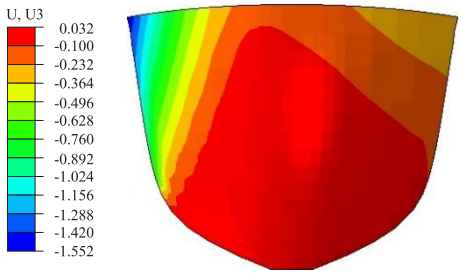

(b) Scenario 2

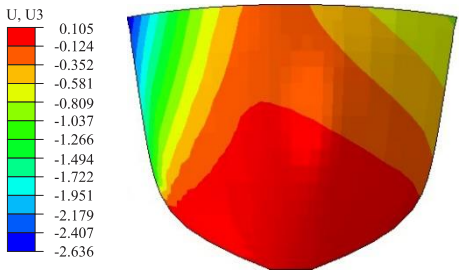

(c) Scenario 3

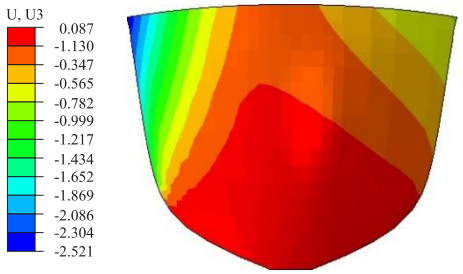

(d) Scenario 4

Fig. 17: The contour of displacement of the dam with wedges at both abutments for different scenarios.

In Figure 18, the tensile damage contours are depicted at the upstream and downstream sides of the dam. Severe damage to the dam body can result from uplift pressure in joints. Damages began at the level of the P1 plane, indicating that the other two planes are open and cracks are growing vertically. As hydrostatic pressure increases, cracks propagate toward the dam's center.

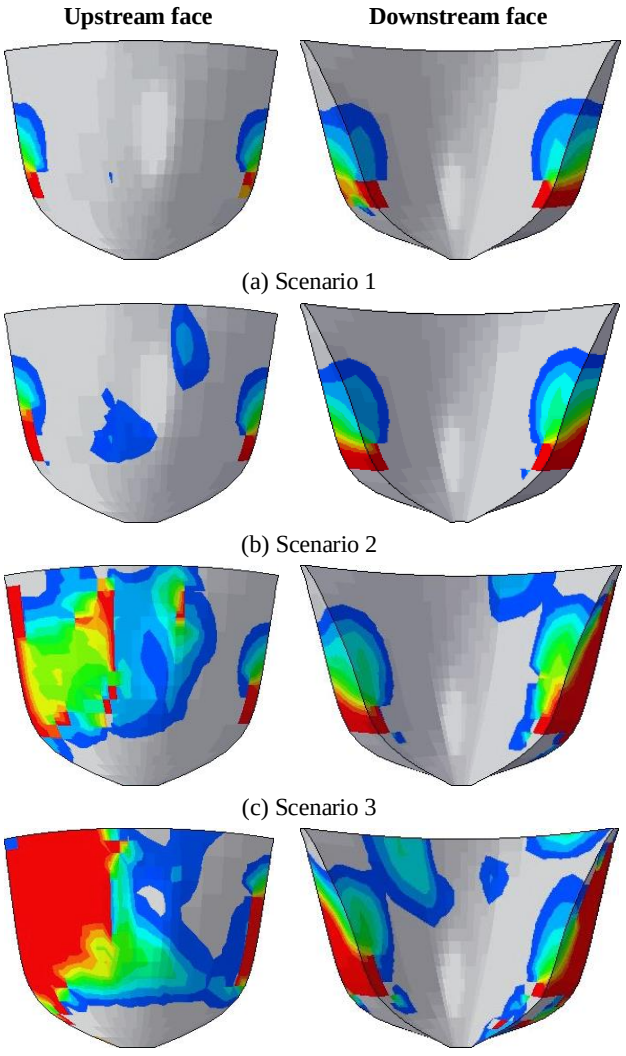

Fig. 18: The contour of tensile damage of the dam having wedges at both abutments for different scenarios.

5. Conclusion

Considering the history of arch dam failure caused by rock wedges' instability indicates that a thorough study of the dams' abutments is vital. These studies were carried out to evaluate the effects of the instability of the abutments on the response of arch dams. Therefore, in this research, an attempt has been made to investigate the seismic stability of dams by considering the placement of these joints. Based on this, the Bakhtiari concrete arch dam with a wedge on each side of the dam was selected, and a three-dimensional finite element model of the dam was developed to simulate the behavior of the dam-reservoir-foundation system. In this finite element model, the foundation is modeled as a mass medium with infinite elements to prevent the wave from returning to the model. A boundary condition was applied at the end of the reservoir to completely absorb the waves moving away from the system.

By considering the wedge joints in the dam foundation in the Abaqus finite element model, the influence of uplift pressure in the joints of the foundation on the response of the dam, including displacements and tensile damages in the dam body were investigated. The results showed that uplift pressure in the joints causes tensile damage in the dam body. Also, with jointed foundation modeling, the dam displacement tends towards the abutments with the wedge. Also, an increase in the pressure in the joints can lead to the creation of tensile damage in the dam body, which can lead to the instability of the dam.

Conflicts of interest

The authors declare that there is no conflict of interest.

References

[1] Takalloozadeh, M., & Ghaemian, M. (2014). Shape optimization of concrete arch dams considering abutment stability. Scientia Iranica, 21(4), 1297-1308.

[2] Shariatmadar, H., & Mirhaj, A. (2011). Dam-reservoir-foundation interaction effects on the modal characteristic of concrete gravity dams. Structural engineering and mechanics, 38(1), 65-79.

[3] Farinha, M. L. B., de LEMOS, J. V., & Maranha Das Neves, E. (2012). Analysis of foundation sliding of an arch dam considering the hydromechanical behavior. Frontiers of Structural and Civil Engineering, 6, 35-43.

[4] Liu, Y. R., He, Z., Leng, K. D., Huang, Y. Q., & Yang, Q. (2013). Dynamic limit equilibrium analysis of sliding block for rock slope based on nonlinear FEM. Journal of Central South University, 20, 2263-2274.

[5] Ghasemof, A., Mirtaheri, M., Mohammadi, R. K., & Mashayekhi, M. R. (2021). Multi-objective optimal design of steel MRF buildings based on life-cycle cost using a swift algorithm. In Structures, 34, 4041-4059.

[6] Mostafaei, H., Mostofinejad, D., Ghamami, M., & Wu, C. (2023). A new approach of ensemble learning in fully automated identification of structural modal parameters of concrete gravity dams: A case study of the Koyna dam. In Structures, 50, 255-271.

[7] Moradi, M., Aghajanzadeh, S. M., Mirzabozorg, H., & Alimohammadi, M. (2018). Underwater explosion and its effects on nonlinear behavior of an arch dam. Coupl. Syst. Mech, 7, 333-351.

[8] Kadkhodayan, V., Aghajanzadeh, S. M., & Mirzabozorg, H. (2015). Seismic assessment of arch dams using fragility curves. Civil engineering journal, 1(2), 14-20.

[9] Salamon, J. W., Hariri-Ardebili, M. A., Estekanchi, H. E., & Mashayekhi, M. R. (2019). Seismic assessment of a dam-foundation-reservoir system using Endurance Time Analysis. In Sustainable and Safe Dams Around the World. CRC Press, 2649-2659.

[10] Shahmohammadi, M. A., Azhari, M., Salehipour, H., Fantuzzi, N., Amabili, M., & Civalek, Ö. (2022). Nonlinear analysis of fiber-reinforced folded shells enriched by nano-additives using a coupled FEM-IGA formulation. Composite Structures, 301, 116221.

[11] Shahmohammadi, M. A., Mirfatah, S. M., Salehipour, H., Azhari, F., & Civalek, Ö. (2022). Dynamic stability of hybrid fiber/nanocomposite-reinforced toroidal shells subjected to the periodic axial and pressure loadings. Mechanics of Advanced Materials and Structures, 1-17.

[12] Gavzan Daroonkola, M. R., & Ahmadi, M. T. (2022). Push-over analysis of concrete gravity dams due to flood inflow. Numerical Methods in Civil Engineering, 6(4), 59-66.

[13] Gavzan, M., & Ahmadi, M. (2022). Numerical Investigation of Static Failure Scenario of Concrete Gravity Dams Considering Water–Crack Interaction. International Journal of Civil Engineering, 1-18.

[14] Pan, J., & Wang, J. (2019). Effect of abutment movements on nonlinear seismic response of an arch dam. Structure and Infrastructure Engineering, 1-15.

[15] Mostafaei, H., Gilani, M. S., & Ghaemian, M. (2018). A comparative study between pseudo-static and dynamic analyses on rock wedge stability of an arch dam. Civil Engineering Journal, 4(1), 179-187.

[16] Mostafaei, H., & Behnamfar, F. (2022). Wedge Movement Effects on the Nonlinear Behavior of an Arch Dam Subjected to Seismic Loading. International Journal of Geomechanics, 22(3), 04021289.

[17] Londe, P. (1973). Analysis of the stability of rock slopes. Quarterly Journal of Engineering Geology and Hydrogeology, 6(1), 93-124.

[18] Londe, P. (1987). The Malpasset dam failure. Engineering Geology, 24(1-4), 295-329.

[19] Wittke, W., & Leonards, G. A. (1987). Modified hypothesis for failure of Malpasset dam. Engineering Geology, 24(1-4), 367-394.

[20] Wittke, W. (1990). Rock Mechanics, Theory and Applications with case histories. Springer-Verlag: Berlin.

[21] Erban, P. J., & Gell, K. (1988). Consideration of the interaction between dam and bedrock in a coupled mechanic-hydraulic FE-program. Rock mechanics and rock engineering, 21(2), 99-117.

[22] Mostafaei, H., Sohrabi Gilani, M., & Ghaemian, M. (2017). Stability analysis of arch dam abutments due to seismic loading. Scientia Iranica, 24(2), 467-475.

[23] Mostafaei, H., Mousavi, H., & Barmchi, M.A. (2023). Finite Element Analysis of Structures by ABAQUS: For Civil Engineers. Simay-e- Danesh Publication : Tehran.

[24] Mostafaei, H., & Behnamfar, F. (2019). Effect of the vertical earthquake component on nonlinear behavior of an arch dam having a foundation with discontinuities. Journal of Numerical Methods in Civil Engineering, 4(2), 69-78.

[25] Lubliner, J., Oliver, J., Oller, S., & Oñate, E. (1989). A plastic-damage model for concrete. International Journal of solids and structures, 25(3), 299-326.

[26] Lee, J., & Fenves, G. L. (1998). Plastic-damage model for cyclic loading of concrete structures. Journal of engineering mechanics, 124(8), 892-900.

[27] Bak, H. M., Kariminia, T., Shahbodagh, B., Rowshanzamir, M. A., & Khoshghalb, A. (2021). Application of bio-cementation to enhance shear strength parameters of soil-steel interface. Construction and building materials, 294, 123470.

[28] Mostafaei, H., Behnamfar, F., Kelishadi, M., & Aghababaie, M. (2021). The effects of friction coefficient on the nonlinear behavior of an arch dam with jointed foundation. Journal of Numerical Methods in Civil Engineering, 5(4), 36-45.

[29] Zhang, Q. L., Li, D. Y., Hu, C., & Hu, L. (2019). Numerical investigation into underwater explosion–resistant performance of an arch dam considering its transverse contraction and control joints. Journal of Performance of Constructed Facilities, 33(6), 04019078.

[30] Mostafaei, H., Behnamfar, F., & Alembagheri, M. (2022). Reliability and sensitivity analysis of wedge stability in the abutments of an arch dam using artificial neural network. Earthquake Engineering and Engineering Vibration, 21(4), 1019-1033.

[31] Sevim, B., Altunşik, A. C., Bayraktar, A., Akköse, M., & Calayir, Y. (2011). Water length and height effects on the earthquake behavior of arch dam-reservoir-foundation systems. KSCE Journal of Civil Engineering, 15, 295-303.

[32] Mostafaei, H., Ghamami, M., & Aghabozorgi, P. (2021). Modal identification of concrete arch dam by fully automated operational modal identification. In Structures, 32, 228-236.

[33] Mostafaei, H., Behnamfar, F., & Alembagheri, M. (2020). Nonlinear analysis of stability of rock wedges in the abutments of an arch dam due to seismic loading. Structural monitoring and maintenance, 7(4), 295-317.

[34] Aghda, S. M. F., GanjaliPour, K., & Esmaeilzadeh, M. (2019). The effect of geological factors on the grout curtain performance analysis of Darian dam using the results of instrumentation data in the first impounding. Journal of the Geological Society of India, 93, 360-368.